Stainless steels: passive film composition, pitting potentials and critical chloride content in concrete

B. Elsener[1),2)], M. Fantauzzi[2)], A. Rossi[2)]

1) ETH Zurich, Institute for Building Materials, CH-8093 Zurich

2) University of Cagliari, Department of Chemical and Geological Science,

Abstract

Stainless steel reinforcing bars show excellent corrosion resistance in concrete structures exposed to harsh environments. Only little information on the surface chemistry of these materials in alkaline media is available. This work reports XPS surface analytical results (thickness, composition of the passive film and of the interface beneath the film) obtained on black steel, FeCr alloys, DIN 1.4301, DIN 1.4462 and the nickel-free DIN 1.4456 after exposure to alkaline solutions simulating concrete. The pitting potentials of the steels could be related to the Cr(III)oxy-hydroxide and Mo(VI) content in the passive film. C_{crit}, the critical chloride content for corrosion initiation in concrete, necessary for life-time predictions can be determined only with time consuming tests, especially for high-alloyed stainless steels. This work reports a correlation between C_{crit} in concrete (made with CEM II A/LL and CEM I) and the pitting potential for carbon steel, Fe12%Cr alloy, DIN 1.4301 and DIN 1.4571 stainless steels. This could allow for the first time a quantitative estimation of C_{crit} for stainless steels in concrete based on short-term solution tests.

1. Introduction

The increasing use of new cement types to reduce CO_2 emission and the requirement for more sustainable structures are challenges for the durability of reinforced concrete structures. The main cause of early damage, loss of serviceability and very high repair costs of reinforced concrete structures is the corrosion of the reinforcement due to chloride ions penetrating into the concrete [1 – 3]. To prevent reinforcement corrosion in marine or road environments splash zone with high chloride concentrations, stainless steels have been proposed since long time [4, 5]. It is well documented that austenitic and duplex stainless steels require up to 10 times higher chloride content to initiate corrosion in concrete and also exhibit much higher pitting potentials than plain carbon steel [6 - 9]. In the past stainless steel reinforcements have been successfully used in a wide range of applications such as bridge engineering, multi-storey car park decks, historic buildings and many others [8 - 11]. A striking example of the use of stainless steels is a pier in the Gulf of Mexico, constructed around 1940. Despite the adverse marine environment, high temperature and humidity and low cover depth no corrosion has been observed so far [12].

Often the high initial costs of traditional stainless steels limit a more widespread use of these materials as reinforcements in practice [13], despite life cycle cost calculations [13, 14] and detailed examination of the additional costs using stainless steel reinforcement [15] have demonstrated that stainless steels would be the material of choice for durable and sustainable structures. To address the problem of material costs, steel companies have developed stainless steel grades with less expensive alloying elements such as lean duplex steels [16] or recently nickel-free stainless steel (obtaining their austenitic structure by adding 18% of manganese). The pitting potential of DIN 1.4456 type nickel-free stainless steels with 18% of manganese has been found to be similar to 18/8/2 CrNiMo steel (DIN 1.4401) and duplex steel DIN 1.4462 in chloride-containing alkaline solutions (pH 13) and in solutions simulating carbonation (pH 9) [17]. A manganese containing stainless steel XM-28 (with 18% Mn but without molybdenum) was found less corrosion resistant compared to 304 or 316LN stainless steels [18].

Whereas the corrosion behaviour of black steel, iron chromium alloys and stainless steels in alkaline solutions and in concrete is broadly described [7 - 16], the formation and analytical characterization of the passive film on the steel surface, responsible for the high corrosion resistance of these alloys in alkaline environment, is by far less known. A recent paper of the

authors in the Encyclopedia of Interfacial Chemistry [19 and literature cited] summarizes the knowledge in the field combining results from electrochemical and surface analytical studies. One of the main results reported was that prolonged immersion (ageing) of Fe-Cr alloys and stainless steels in alkaline solution improves the resistance to pitting, mainly because the chromium oxide content in the passive film increases and the content of Fe^{2+} defects decreases. This was reported in detail for Fe15Cr alloy, DIN 1.4301 austenitic stainless steel and DIN 1.4462 [17, 20] and for the nickel free manganese steel DIN 1.4456 [17, 21] exposed to various alkaline environments simulating concrete pore solutions.

Based on our work and on literature data this paper intends to address two important issues regarding the corrosion resistance of stainless steel reinforcements: first, the rationalization of electrochemical data, paying special attention to the pitting potentials from solution experiments, with the results of ex-situ XPS surface analysis (chemical state and composition of the surface film) formed for different alloy / solution systems. As the stainless steels will be used as reinforcements in concrete, the second point is the attempt to establish a correlation between the pitting potentials obtained in short-term solution tests with the critical chloride content for corrosion initiation in concrete that is usually determined with time consuming but more realistic tests. This will enable an informed choice of the materials and might open new perspectives for tuning the physicochemical properties of steels.

2. Materials and methods

Materials:

The composition of the materials investigated in this work is provided in table 1 together with the PRE (pitting resistant equivalent or Wirksumme, calculated as %Cr + 3.3*%Mo). The composition was checked with energy-dispersive X-ray analysis (EDX) [23]. In order to ensure reproducible results, the surface of the alloys was first ground with emery paper in water and then mirror-like polished using diamond pastes up to 1 μm (Struers, Bellerup DK) in ethanol (absolute ethanol supplied by Carlo Erba, Italy) Samples were washed with ethanol and dried in an argon stream. At least two independent measurements were carried out in this study for each solution investigated. More details are reported in [17, 20-23].

Table 1:　　　Composition (wt.%) of the steels and pitting resistant equivalent (PRE), or *Wirksumme*, calculated as %Cr + 3.3*%Mo

Element	Cr	Ni	Mn	Mo	other	AISI equivalent	PRE
1.0037	-	-	-	-		1015	0
Fe15Cr	15	-	-	-	-		15
1.4301	18.1	8.7	-	< 0.1	S 0.003	304	18
1.4462	21.8	5.6	-	2.9	S 0.005	318 LN	32
1.4456	17.9	0.2	18.4	1.9	S 0.004		24

Solutions:

The mechanically polished samples were exposed to different solutions simulating the concrete pore environment:

1.　　　0.1 M NaOH, pH 13
2.　　　synthetic pore solution, 0.25 M KOH + 0.02 M NaOH + 0.01 M Na_2SO_4 + 0.0001 M $Ca(OH)_2$, pH 13.2

The synthetic pore solution was based on results of pore solution expression of mortar with CEM I w/c ratio 0.5 [3, 24]. Aggressive conditions were created by adding chloride ions in a range from 0.1 to 5 M NaCl to these alkaline solutions. All reagents were of at least ACS grade and the solutions were prepared with distilled water having a conductivity of 0.8 μS/cm. All solutions were stored in a vessel of 1 dm3 and de-aerated for one day with argon gas. Argon bubbling was prolonged during the measurements. The oxygen content of the solution was checked with the instrument HD3409.2 (Deltaohm) and found to be 0.29 ± 0.06 mg/dm^3 [23].

Electrochemical tests:

A 273A potentiostat/galvanostat (EG&G PAR, Oak Ridge, Tennessee, USA) was used to perform the open circuit potential measurements using a three-electrode electrochemical cell.. An Autolab potentiostat/galvanostat (ECO Chemie NL) was exploited for recording

polarization curves (scan rate was 0.2 mV/s) and the potentiostatic tests at -0.1 V SCE. All potentials are referred to the saturated calomel electrode (SCE).

XPS Surface analysis and data processing:

At the end of the electrochemical tests (OCP and potentiostatic test) the samples were washed with distilled water, dried in a stream of Argon and transferred in less than one miute to the fast entry lock of the spectrometer with a vacuum of ca. 10^{-5} Pa.

XPS analysis was performed with a Theta Probe ARXPS spectrometer (Thermo Fischer Scientific) using the AlKα source at 70 W. The analyzer was operated in the fixed analyzer transmission mode. Three points with a spot size of 300 μm were analyzed on each sample. The pump system consisted in two turbo-molecular pumps, one operating in the fast entry lock chamber, one in the analysis chamber. The residual pressure in the UHV chamber was always lower than $5*10^{-7}$ Pa.

The binding energy scale was calibrated using the standard procedure [25]. Sample charging was compensated referring all binding energies to the C1s signal at 285 eV. Data processing is described in detail elsewhere [22, 23, 26]. Thickness and composition of the passive films formed on the three alloys and the composition of the metal interface beneath the film have been calculated using a three-layer model [27]. The calculations were based on the integrated XPS intensities of the different components that were corrected for Scofield's photo-ionization cross-sections [28], the instrument transmission function and the inelastic mean free path (IMFP).

3. Results

3.1 Open circuit potential

The open circuit potentials of the mechanically polished alloys in the alkaline solutions were in the range of − 500 ± 50 mV SCE after immersion and increased asymptotically with time [17, 20, 21]. The OCP values at the end of immersion are summarized in Table 2. The stainless steels show slightly more positive OCP values compared to the black steel and the Fe15Cr model alloy. No significant difference is observed comparing the 0.1 M NaOH solution with the synthetic pore solution. All the samples were analysed by XPS surface analysis at the end of the test.

Table 2: Values of the open circuit potential of the samples after immersion of 24 h in 0.1 M deaerated NaOH and synthetic pore solution

Material	0.1 M NaOH	synthetic pore solution
1.0037	- 0.35 ± 0.03	-
Fe15Cr	-0.34 ± 0.03	-0.35 ± 0.03
1.4301	-0.32 ± 0.01	-0.34 ± 0.02
1.4462	-0.28 ± 0.02	-0.32 ± 0.02
1.4456	-0.34 ± 0.02	-

3.2 Anodic polarization curves

Examples of the dynamic anodic polarization curves of the different materials in the two alkaline solutions tested with up to 5 M NaCl added are shown in Figure 1, additional data were published [17, 20, 21]. All samples show a rapidly increasing anodic current density after the OCP reaching a dynamic passive current density of ca.1-2 $\mu A/cm^2$ indicating passivation. All the alloys with chromium exhibit a maximum of the current density at around + 100 mV SCE due to the Cr^{3+} to Cr^{6+} transformation.
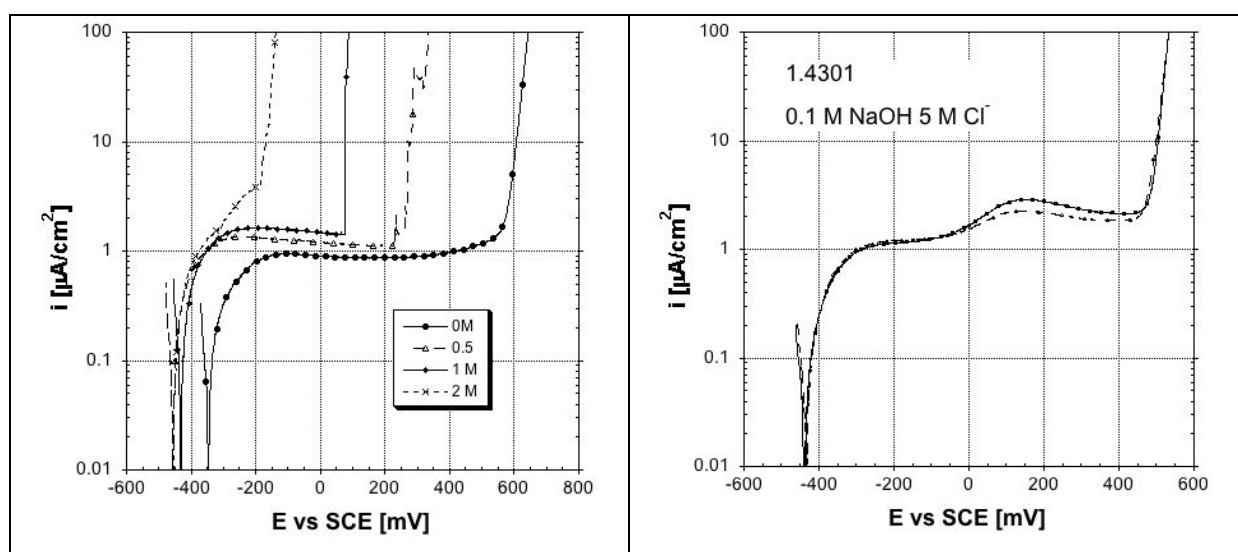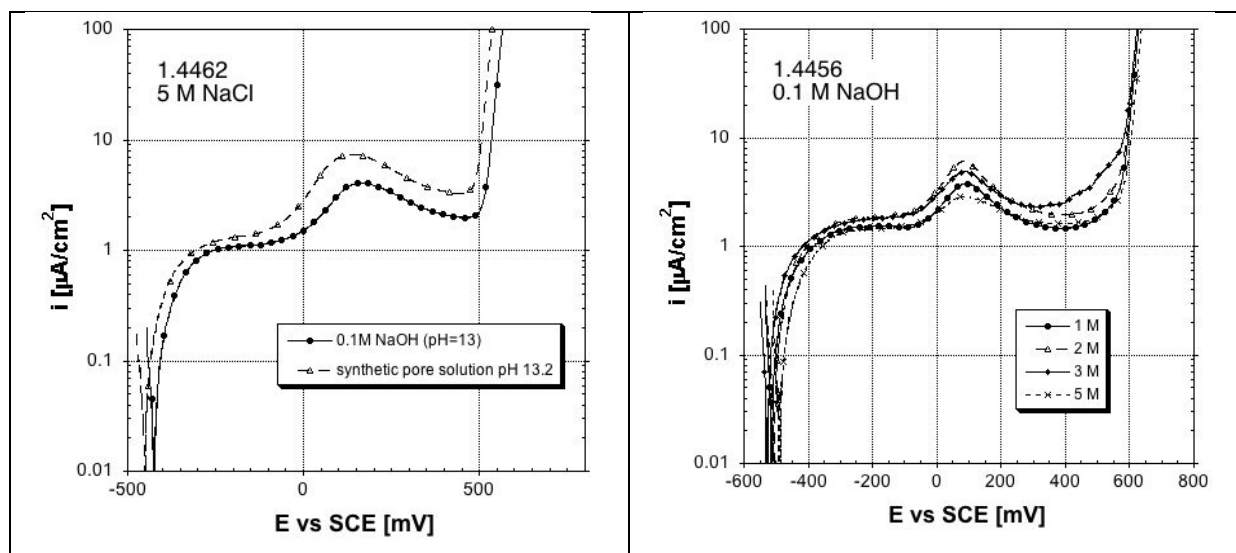
Figure 1: Anodic polarization curves of a) black steel in 0.1 M NaOH + NaCl, b) 1.4301 stainless steel in 0.1 M NaOH + 5M NaCl, c) 1.4462 stainless steel in 5M NaCl containing 0.1 M NaOH and synthetic pore solution, d) 1.4456 stainless steel in 0.1 M NaOH + NaCl

From Fig. 1 it can be noted that in 0.1 M NaOH all the stainless steels tested are in the passive range and reach the oxygen evolution potential up to 5 M NaCl added. The same result was found for the slightly more alkaline pore solution. Onset of pitting corrosion was found for black steel (Fig. 1a) at 0.5 M NaCl and for Fe15Cr model alloy at chloride contents higher then 0.5 Mol/dm^3. The stainless steel 1.4301 in 0.1 M NaOH with 5 M NaCl showed no pitting corrosion in 4 out of 8 replica experiments [21], two experiments showed pitting at +200 mV SCE and other two at +400 mV SCE. The pitting potentials determined for the different materials in the alkaline solutions were reported in ref. [21].

3.3 Potentiostatic tests

The potentiostatic polarization tests at -0.1 V SCE were performed to examine the formation of the passive film over time in a chloride free 0.1 M NaOH and pore solution. The results (Figure 2) show that all the alloys exhibit a continuous decrease of the current density following a power law with approximately a slope of -0.8, close to the theoretical value of -1. The current densities are highest for the Fe15Cr model alloy, about a factor 2 – 3 lower for the stainless steel 1.4301 and for the duplex 1.4462. After one day the passive current density is in the order of 10 – 20 nA/cm^2. All the samples were analysed by XPS at the end of the test.
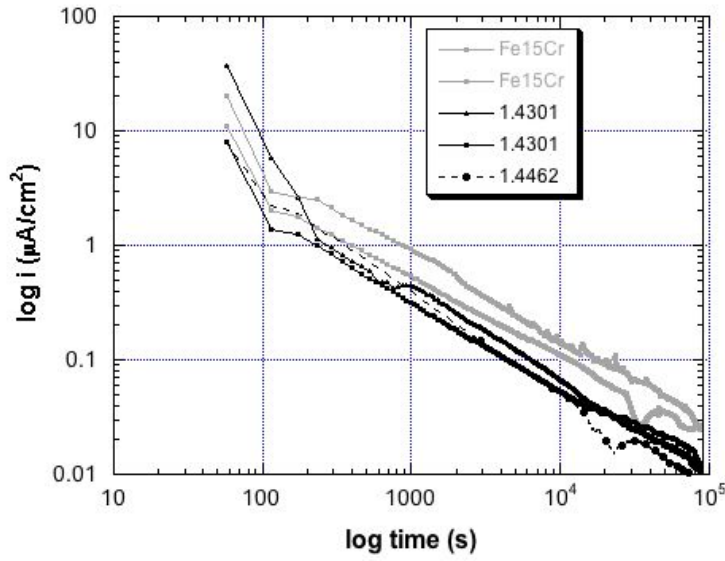
Figure 2: Current density vs time curves for the potentiostatic polarization at -0.1 V SCE of Fe15Cr, DIN 1.4301 and DIN 1.4462 alloys in 0.1 M NaOH.

3.4 X-ray photoelectron spectroscopy results

The surface of the materials was analysed after exposure at the OCP and after potentiostatic polarization at -0.1 V SCE in 0.1 M NaOH and in the synthetic pore solution. In this work only examples of the XPS spectra are presented, the full details are provided in [17, 20 – 23]. The survey spectra (not shown) only exhibit x-ray photoelectron and Auger induced signals from the alloy constituents, carbon and oxygen that are due to the sample exposure to the solution and to the atmosphere. No traces of ions from the solutions (Na^+, Ca^{2+}, Cl^-) were revealed.
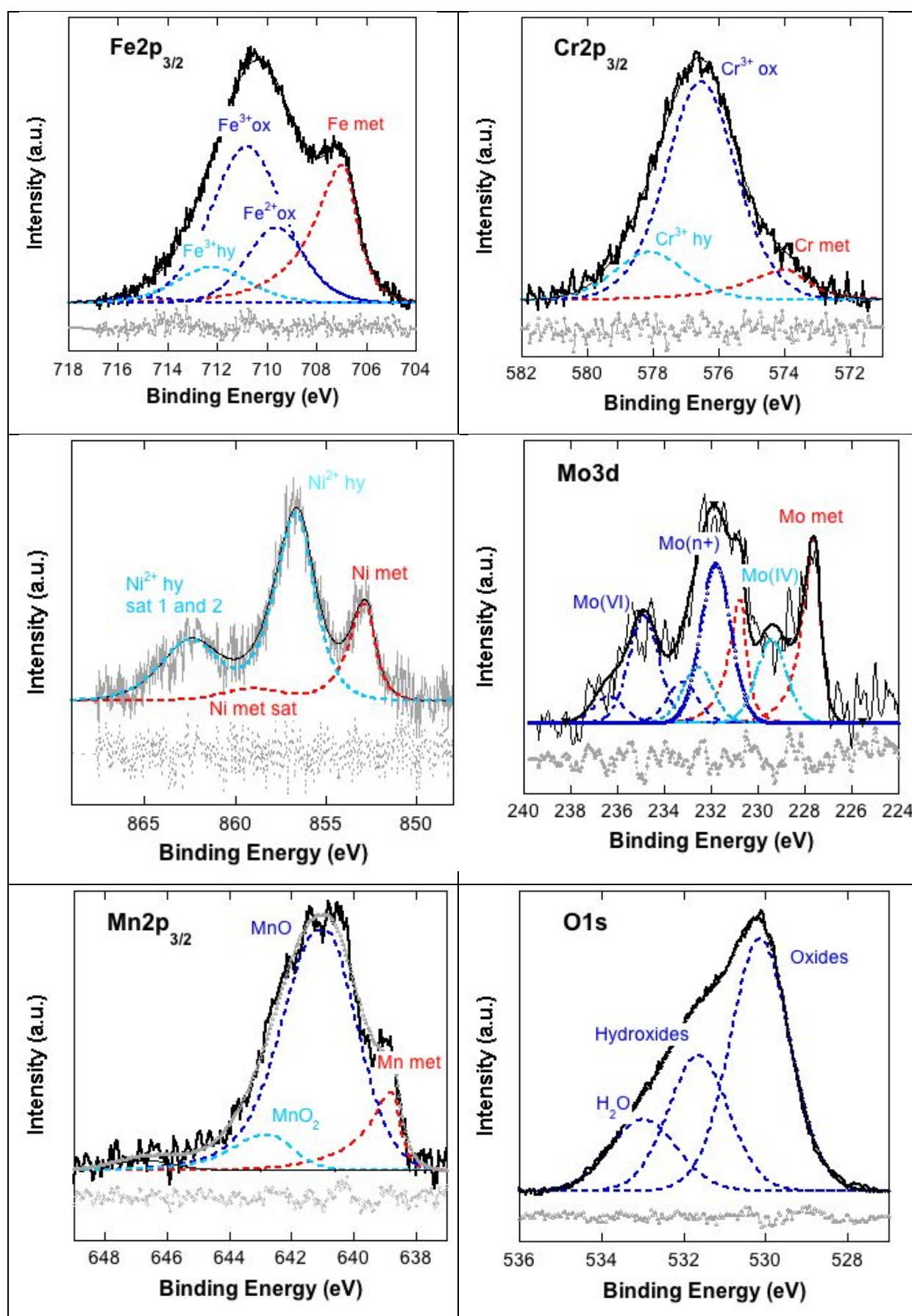
Figure 3: XPS high-resolution spectra of the alloy elements and of the oxygen in the passive films formed after exposure to alkaline solution 0.1 M NaOH after background subtraction and curve fitting.

High-resolution spectra

High-resolution spectra were recorded of the most intense lines of iron, chromium, nickel, manganese and molybdenum (according to the composition of the alloy) and oxygen. Figure 3 shows examples of the photoelectron signals after background subtraction and curve fitting. The difference between the fitted envelope of the spectrum and the experimental data is shown below the spectrum as an indication of the quality of the fit.

The *iron Fe2p $_{3/2}$ spectrum* (Fig. 3a) is composed of four components: metallic iron at 706.8 ± 0.1 eV, iron(II)oxide at 709.6 ± 0.2 eV with its satellite at +5.5 eV and iron(III)oxide at 710.8 ± 0.2 eV. The binding energies and peak widths are in agreement with a study on iron oxides [29]. The fourth component in the iron spectrum has been attributed to iron(III)oxy-hydroxide. More details are given in [19].

The *chromium Cr2p $_{3/2}$ spectrum* (Fig. 3b) contains a low intensity metallic component (573.9 eV ± 0.1 eV, chromium(III) oxide at 576.5 ± 0.2 eV and chromium(III) hydroxide at 578.0 ± 0.2 eV. The *Ni2p $_{3/2}$ spectrum* (from the 1.4301 stainless steel) shows the presence of metallic and oxidized nickel, both with the corresponding satellites at high binding energy values (Fig. 3c). Metallic nickel was detected at 852.8 ± 0.1 eV with a satellite at +5.8 eV, the oxidized component was found at 855.7 ± 0.2 eV with two intense satellites at +0.75 and + 6.0 eV. All the components in the *molybdenum Mo3d spectrum* (Fig. 3d) show the characteristic doublet structure, difference between 5/2 and 3/2 peak was 3.2 eV, the intensity ratio 3 : 2. The spectrum is complex because molybdenum may be present in the passive layer in different oxidation states. The metallic signal Mo3d$_{5/2}$ was found at 227.7 ± 0.1 eV, the oxidized components at 230.6 ± 0.2 eV and 223.3 ± 0.2 eV, assigned to Mo(VI) and Mo(IV). The *manganese Mn2p $_{3/2}$ spectrum* (Fig. 3e) shows the presence of metallic and oxidized manganese, both with associated satellite structure. Metallic manganese was detected at 638.7 ± 0.1 eV, the component at 642.0 ± 0.2 eV was assigned to MnO_2, another low intensity signal might be due to multiplet splitting [21]. In the *oxygen O1 spectrum* (Fig.3f) three contributions were found: the highest intensity signal at 530.1 ± 0.1 eV corresponding to oxygen in the metal oxides, the second at 531.7 ± 0.2 eV assigned to metal-bonded hydroxide groups and the third at 533.0 ± 0.2 eV to adsorbed water.

Examining the high-resolution spectra, no changes in the binding energies of the metallic elements and oxygen with immersion time were observed [20 – 23]. However, changes in the intensity of the iron(II) and iron(III) signals were found. The Fe(II) component in the iron signal diminished upon immersion time in all the alloys [19 – 21], reducing the amount of defects in the passive film [17, 19] as it is also reported after potentiostatic passivation [19].

Quantitative analysis – film thickness and composition

Film thickness, film composition and also the composition of the metallic interface beneath the passive film were evaluated quantitatively based on the three-layer model [19, 27]. This quantitative calculation method provides average composition of the three layers (hydro-carbon contamination, oxide-hydroxide passive film, metal beneath the passive layer). In reality, in depth composition gradients are present as shown with angle-resolved XPS for the manganese DIN 1.4456 steel [21]. The signals originating from Fe(III) oxide, Cr(III) oxide, Mn(II) oxide and the oxide component in the O1s spectra decreased with emission angle, indicating that these oxides are located in the inner part of the film whereas the hydroxide components are located in the outer part of the passive film [21].

Thickness of the passive film and its composition of the alloys determined after 1d of immersion in alkaline solution (0.1 M NaOH) are shown in Table 4. Only the duplex steel 1.4462 and the nickel free steel 1.4456 show a chromium oxide/hydroxide content near to or higher than 50% (the limit indicated for stable passivity), the two iron-chromium alloys and the stainless steel 1.4301 show a chromium oxide/hydroxide content in the range from 34 to 45%. The austenitic DIN 1.4301 shows a marked enrichment of the nickel oxide content in the film (up to 15%) [20, 22]. In contrast, the nickel-free stainless steel 1.4456 shows a slight depletion of oxidized manganese in the film [21, 23]

Table 4: thickness (nm) and composition (weight %) of the passive film formed on the alloys after 1d immersion in 0.1 M NaOH. Fe10Cr model alloy added for comparison [30].

Material	Thickness (nm)	Feox (wt%)	Crox (wt%)	Niox (wt%)	Mnox (wt%)	Moox (wt%)
Fe10Cr	2.6± 0.2	66	34	-	-	-
Fe15Cr	3.6 ± 0.2	55	45	-	-	-

1.4301	3.9 ± 0.2	43	46	15	-	-
1.4462	3.9 ± 0.2	38	55	4	-	4
1.4456	3.1	32	48	-	14	5

Evolution with time of immersion

The passive film of iron, iron-chromium alloys stainless steels show an evolution of the composition, chemical state and thickness as presented in [19 and literature therein]. The thickness of the passive film of the alloys is increasing linearly with logarithm of immersion time [17, 19 – 23]. The passive film composition changes with immersion time: an increase in chromium oxy-hydroxide and a decrease in the content of iron oxide are observed [17, 19 – 23]. As shown in Figure 4, the iron oxide content decreases with time of immersion, for Fe10Cr and Fe15Cr model alloys it does not decrease below 50% even after 3 days of immersion in alkaline solution 0.1 M NaOH (Figure 4). For the two stainless steels 1.4462 and 1.4456 instead the iron oxide content in the passive film continues to decrease.
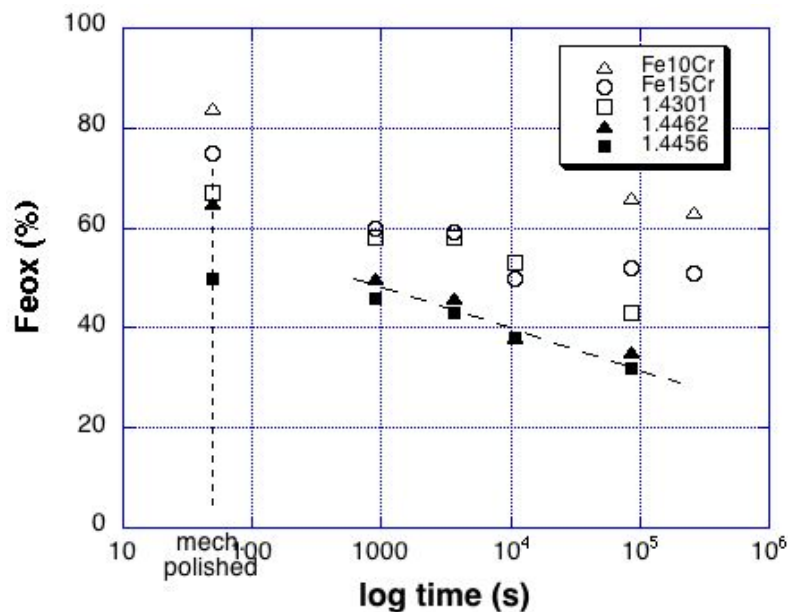

Figure 4:Evolution with time of the iron oxide content in the passive film of the alloys studied, immersion in 0.1 M NaOH. Fe10Cr alloy is given for comparison [30].

The evolution of the total Fe(II) content in the passive films (calculated as the percentage of Fe(II) respect to the iron oxide content multiplied by the iron oxide content in the film) of the different alloys with time of immersion in alkaline solution is shown in Figure 5. Interesting

to note that after 1 day and 3 days of immersion the total Fe(II) content in the passive film reaches similar and low values of 3 – 5% in all the alloys studied.
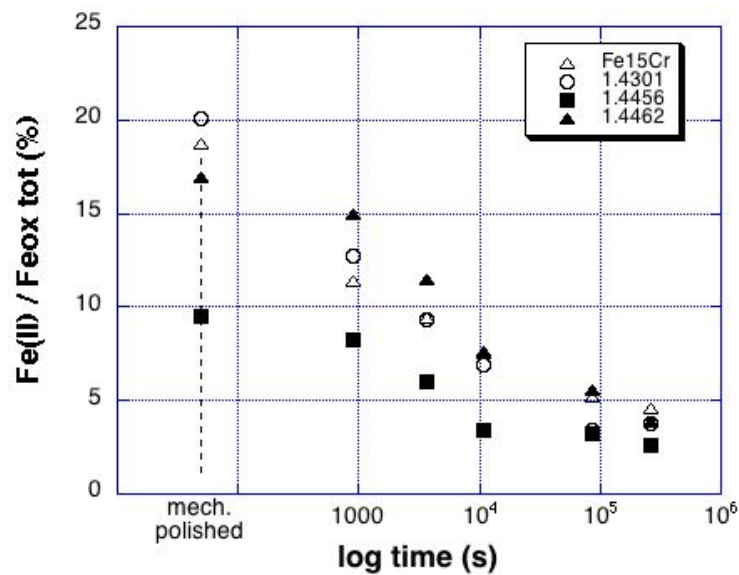

Figure 5: Evolution with time of immersion of the total Fe(II) content in the passive film of the alloys studied.

Comparison of surface films formed after exposure at OCP and potentiostatic tests

Based on the integrated intensities determined from curve fitting of the high-resolution spectra and the evaluation with the three-layer model [19, 27] the thickness and composition of the surface films formed were determined. The comparison of the results obtained on the alloys Fe15Cr, DIN 1.4301 and DIN 1.4462 after 1d open circuit exposure (Table 2) and after 1d potentiostatic polarization at -0.1 V SCE (Figure 2) is shown in Table 5.

Table 5: Compositions of the surface films (weight%) on the alloys after 1 d immersion in deaerated 0.1 M NaOH

Material	Solution	OCP exposure				Potentiostatic -0.1 V SCE			
Material	Solution	Feox	Crox	Niox	Moox	Feox	Crox	Niox	Moox
Fe15Cr	0.1 M NaOH	53	47	-	-	59	41	-	-
	pore solution	56	44	-	-	54	46	-	-
1.4301	0.1 M NaOH	42	43	15		44	40	16	

	pore solution	39	49	12		38	39	23	
1.4462	0.1 M NaOH	36	58	4	3	38	57	5	5
	pore solution	40	52	4	4	30	52	14	4

First an excellent agreement of the passive film composition formed in the two alkaline solutions can be observed for the open circuit exposure, in agreement with the very similar values of the open circuit potential (Table 2). The chromium oxy-hydroxide content in the passive film increases from 45% for the Fe15Cr alloy and the stainless steel 1.4301 up to 55% for the 1.4462 duplex stainless steel. The same trend can be observed in the passive film formed after 1d potentiostatic polarization for one day in the two alkaline solutions. The results confirm the evolution of the passive film upon immersion time at the OCP (Fig. 4).

Metallic interface beneath the passive film

Most quantitative analysis of oxy-hydroxide surface films and passive films formed focus on the composition of the surface or passive film itself. Very often, the metallic interface directly beneath the layer is not considered or is assumed to have the bulk composition. As many surface analytical studies of the authors on a great variety of systems instead show, the composition of the metallic interface is markedly different from the bulk composition. This has been confirmed by results obtained using hard x-rays photoelectron spectroscopy [31]. This might be important when considering that chloride ions, after having destroyed the passive film, reach this metal layer. For the alloys studied in this work the interface composition is given in Table 6.

Table 6: Compositions of the metallic interface beneath the passive film formed after 1d exposure at OCP in the alkaline solutions for the alloys studied [17, 19]. Fe10Cr model alloy is provided for comparison [30].

Material	Fe	Cr	Ni	Mn	Mo
Fe10Cr	93 ± 4	7 ± 2	-	-	-
Fe15Cr	86 ± 8	14 ± 2	-	-	-
1.4301	50 ± 3	12 ± 2	38 ± 3	-	-
1.4462	57 ± 4	10 ± 2	27 ± 3	-	6 ± 1
1.4456	73 ± 3	15 ± 2	-	9 ± 2	2 ± 0.5

The interface composition differs from the nominal bulk composition of the alloys. It is important to notice is the very strong enrichment of nickel up to nearly 40 and 30% respectively beneath the passive film in the stainless steels 1.4301 (8% of Ni in the bulk) and 1.4462 (6% in the bulk). Correspondingly the amount of chromium beneath the film is much lower. The interface of the DIN 1.4456 stainless steel is strongly depleted in manganese (only 9%). Note that the values listed in Table 6 are averaged compositions, in reality a composition gradient can be predicted at the interface, thus directly beneath the film the enrichment / depletion might be more pronounced. Due to the limited escape depth of the photoelectrons in XPS a higher thickness of the oxidic surface film will lead to more pronounced enrichment/depletion at the interface.

4. Discussion

The results obtained combining electrochemical and surface analytical investigations confirm that stainless steels are well suited to achieve a maintenance free service life of reinforced structures exposed to chloride salts such as marine structures, bridges or parking decks. In the following discussion the results will be compared with literature work

4.1 Comparison of pitting potentials with results from literature

Various literature studies reported pitting potentials for reinforcing steels in alkaline, chloride containing solutions that allow a comparison with the results of the present authors (Figure 6).
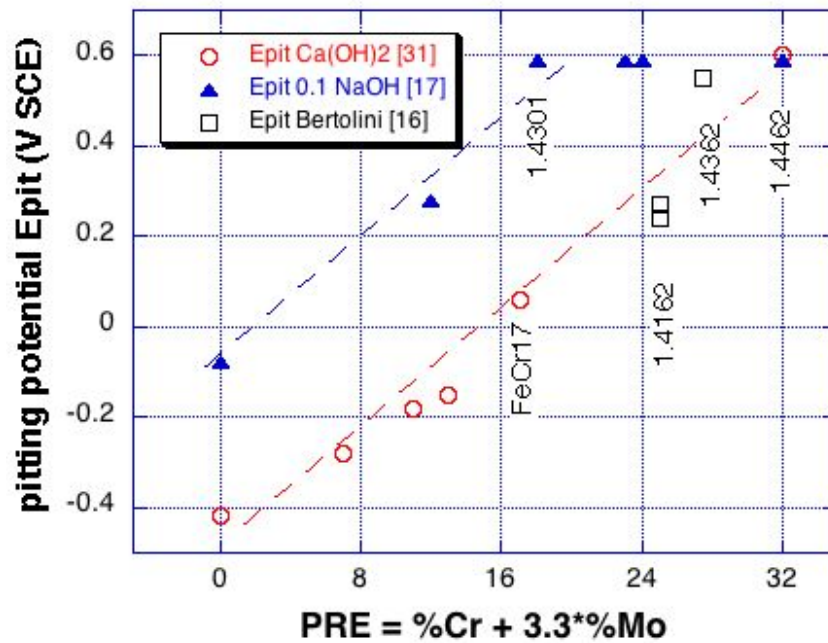
Figure 6: Pitting potentials of steels and stainless steels determined in sat. Ca(OH)$_2$ [16, 32] and in 1 N NaOH [17] with 5% Cl$^-$ added. Poteniodynamic polarization.

The pitting potentials E$_{pit}$ obtained with potentiodynamic tests on black steel, low-alloyed chromium steels and stainless steels in saturated Ca(OH)$_2$ solution with 5% chloride (ca. 1.5 M/dm^3) are reported in [32]. E$_{pit}$ shows an approximately linear increase with the pitting resistance equivalent (PRE) calculated as PRE = %Cr + 3.3*%Mo. Black steel showed a pitting potential of -0.42 V SCE, the duplex stainless steel DIN 1.4462 did not show pitting and reached the oxygen evolution potential at +0.6 V SCE. Included in Fig. 6 are also pitting potentials of three lean duplex steels determined in Ca(OH)$_2$ solution with the same chloride concentration [16].

In comparison, pitting potentials determined by the authors [17] in 0.1 M NaOH are much more positive due to the higher pH of the solution. The sequence in agreement with the PRE is found also for this series of data. Note that stainless steels 1.4301 and higher reach the oxygen evolution potential. In order to rank the pitting resistance of the stainless steels, the chloride containing less alkaline saturated Ca(OH)$_2$ solution should be used.

4.2 Relation to results from surface analysis

Compared to electrochemical tests performed in solutions, surface analytical studies of stainless steels in alkaline solutions are rare [see 19 and literature cited therein]. In this study the thickness and composition of the passive film formed after exposure of the alloys studied

to alkaline solutions (Table 4) as well as the composition of the interface beneath the film (Table 6) are reported. An attempt was made to relate these surface analytical results to the pitting potentials determined in solutions. Figure 7 shows that the pitting potentials determined in chloride containing saturated $Ca(OH)_2$ solution [32] can be rationalized by the passive film composition with a "composition index", obtained by calculating %Cr(ox) + 3.3%Mo(VI).

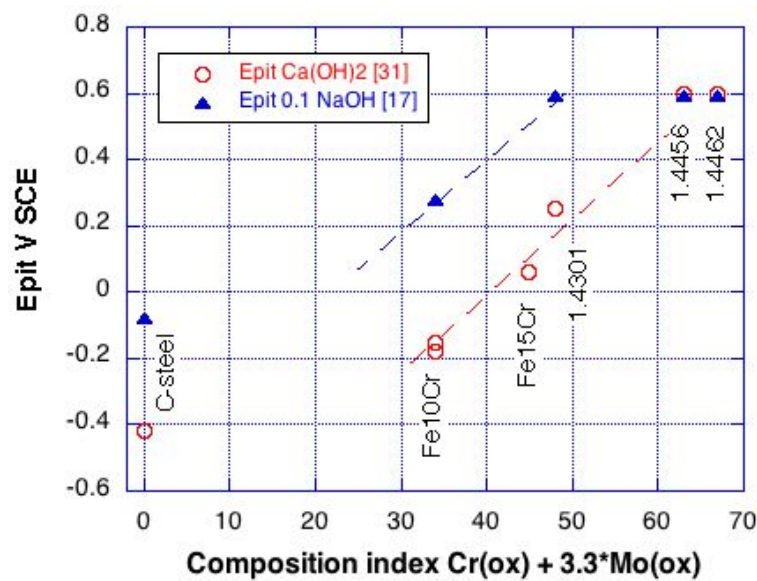
Figure 7: Pitting potentials of steels and stainless steels determined in saturated $Ca(OH)_2$ [32] and in 0.1 M NaOH [17] each with 5% of chlorides as a function of the passive film composition obtained after 1 d exposure of the steels to alkaline solution (Table 4).

This relation obtained by combining two different data sets from different research work may be criticized: the steel surface preparation and the exact steel composition might not be identical, solution pH is different, the composition of the interface beneath the passive film is not considered, pitting potentials may scatter and are statistically distributed – but in this way a clear and quantitative relation can be established between XPS surface analysis results and pitting potentials that goes beyond simple ranking of the steels, covering the range from low grade Fe10Cr alloy to high-grade DIN 1.4462 stainless steels. Pitting potentials determined in the highly alkaline 0.1 M NaOH solution (pH 13) are more positive, but this solution seems less appropriate because the high alloyed stainless steel reach the oxygen evolution potential.

4.3 Relevance of laboratory tests for practice

In a reinforced concrete structure the steel is embedded in a cementitious matrix and has a prescribed minimum distance from the surface (cover depth). Chloride ions from the harsh environment have first to penetrate into the concrete and reach the steel in sufficiently high concentration, the critical chloride content C_{crit}. It is well known that C_{crit} is a system parameter, influenced by factors related to the steel concrete interface [33], by the size of the samples used in the tests [34] and that for these reasons C_{crit} can not be considered as a fixed value but a statistical distribution with mean value and standard deviation has to be applied. For normal black steel reinforcement in harsh environment the time to corrosion onset can last 20 – 50 year. When using stainless steels as reinforcement, corrosion initiation is expected not to occur in the planned service life of the structure (that might exceed 100 years). This implies that the critical chloride content C_{crit} should be higher than the expected chloride content at the depth of the reinforcement at the end of the design service life.

A test procedure to determine C_{crit} should – ideally – simulate the conditions in practice: reinforcement embedded in concrete with a realistic steel/concrete interface, same exposure conditions and same chloride content in the (splash) water. RILEM TC committee made attempts to develop such a test [35]. An interesting way to determine realistic C_{crit} values, taking concrete cores with a non-corroding reinforcement from real structures and expose and test the cores in the laboratory was proposed and successfully applied [36].

The main problem in all the tests is the long duration, becoming even more crucial when testing more corrosion resistant reinforcements. Several options exist to accelerate the chloride penetration (and thus greatly reduce the test duration): reducing the cover depth, increase the chloride concentration in the (splash) water, frequent wetting and drying, and increase the flux of water and chlorides in the concrete. Such a test setup and procedure with cover depth of 15 mm, chloride concentration of 3 Mol/dm^3 and a fan to dry out the concrete surface was used in a study aimed to investigate the corrosion resistance of stainless steels reinforcement in concrete [37]. Despite these accelerating conditions the test duration was in the range of 6 month to one year.

The C_{crit} results obtained in concrete made with CEM II-A/LL (and a few in CEM I) are shown in Figure 8, plotted versus the pitting potential in solution. A good correlation was obtained for the data set with four steels tested in CEM II, but also for CEM I. For the first time the results of the critical chloride content for the corrosion onset of chromium steels and stainless steels in concrete (determined with realistic, time consuming tests [36]) can be

related to pitting potentials obtained in rapid potentiodynamic tests in solution. This result could allow predicting realistic C_{crit} in concrete from rapid potentiodynamic tests performed in solution.
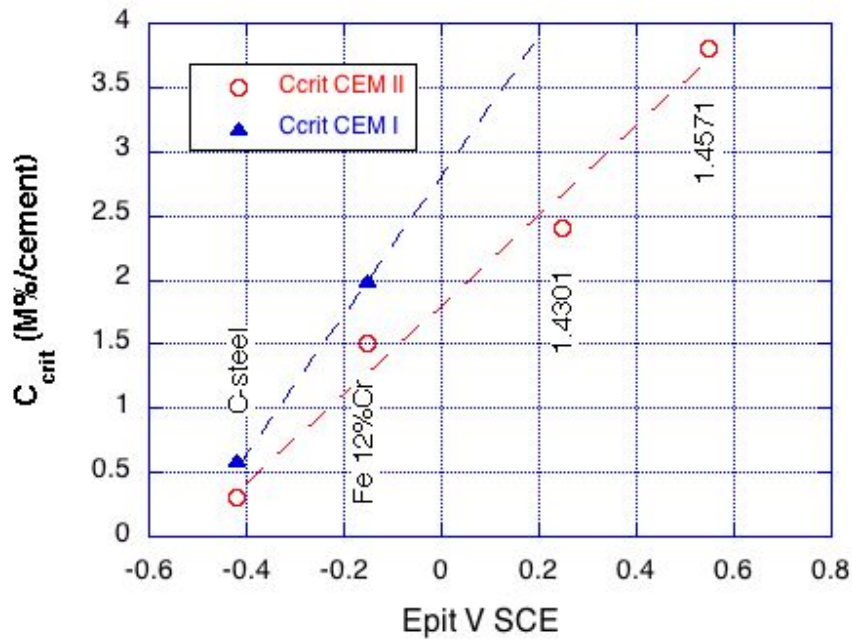

Figure 8: Critical chloride content for corrosion initiation in concrete obtained from long-term tests [37] versus pitting potentials from potentiodynamic polarization tests [32]

Final remarks

The correlation between C_{crit} and the pitting potential (Fig. 8) obtained from two different (and limited) data sets should be examined critically. There is a lack of information on the possible scatter of both, C_{crit} and E_{pit}, that are parameters related to the stochastic process of pit initiation. Nevertheless, compared to a simple application of the concept of PRE value, the pitting potentials determined in solution (form [32]) give a better prediction of C_{crit} in concrete.

5. Conclusions

This study combines results of XPS surface analysis of steel, FeCr alloys and stainless steels exposed to alkaline solutions, pitting potentials of our own work and from literature determined in chloride containing alkaline solutions and relates these data to values of C_{crit} determined on steel, Fe12 Cr alloy and stainless steels in concrete. The following conclusions can be drawn

- In order to determine pitting potentials of steel, FeCr alloys and the full range of high-alloyed stainless steels, a solution of saturated $Ca(OH)_2$ with about 2 moles/dm^3 chloride ions should be chosen. In a more alkaline solution of 0.1 M NaOH even with 5 moles/dm^3 of chlorides, stainless steel grades higher alloyed then DIN 1.4301 reach the oxygen evolution potential.

- Pitting potentials from own work and from literature data of FeCr alloys and stainless steels can be related to a "composition index" of the passive film calculated as %Cr(III) + 3.3 * % Mo(VI), thus taking into account the content of chromium (III) oxy-hydroxide and of Mo(VI) oxides.

- A first attempt has been made for correlating the results of the critical chloride content C_{crit} for the corrosion onset of steel, Fe12Cr alloy, 1.4301 and 1.4571 stainless steels in concrete (determined with realistic, but time consuming tests [37]) with a short-term (pitting potentials obtained in alkaline solution [32]).

- Additional work is required to establish the scatter (mean value and standard deviation) of both C_{crit} in concrete and E_{pit} in solution in order to substantiate the relation.

Literature references

[1]   ACI Committee 222, Corrosion of Metals in Concrete, Detroit (1996) American Concrete Institute.

[2]   B. Elsener, Corrosion of Steel in Concrete, in *Corrosion and Environmental Degradation* Vol. 2 p. 389 – 436, Materials Science and Technology Series, WILEY VCH (2000).

[3]   L. Bertolini, B. Elsener, P. Pedeferri, E. Redaelli, R. Polder, Corrosion of Steel in Concrete – Prevention, Diagnosis, Repair, Wiley VCH 2nd edition (2013).

[4]   D.B. Mac Donald, M.R. Sherman, D.W. Pfeifer, Y.P. Virmani, Concrete International, May 1995.

[5]   Guidance on the use of stainless steel reinforcement, The Concrete Society, Technical Report No. 51 (1998).

[6]   Stainless Steel in Concrete, U. Nürnberger (Ed.), EFC Publication Nr. 18, The Institute of Materials, London (1996).

[7]   L. Bertolini, P. Pedeferri, Corros. Rev. 20 (2002) 129.

[8]   C.M. Hansson, Corrosion of stainless steel in concrete, in "Corrosion of Steel in Concrete Structures", ed. A. Poursaee. Woodhedad Publishing, Elsevier (2016)

[9]   F. Lollini, M. Carsana, M. Gstaldi and E. Redaelli, Corros. Rev. 37 (2019) 3 - 19

[10] C.J. Abbott, Concrete 31, 5 (1997) 28.

[11] W.H. Hartt, R.G. Powers, D.K. Lysogorski, V. Liroux, Y.P. Virmani, *Corrosion Resistant Alloys for Reinforced Concrete*, FHWA-HRT-07-039, July 2007. http://www.fhwa.dot.gov/bridge/pubs/07039/07039.pdf

[12] P. Castro-Borges, O.T. de Rincón, E.I. Moreno, A.A. Torres-Acosta, M. Martínez-Madrid, A. Knudsen, Mater. Performance 41, 10 (2002) 50.

[13] M. Yunovich, N.G. Thompson, Y.P. Virmani, Life Cycle Cost Analysis for Reinforced Bridge Decks, paper 03309 presented at CORROSION/03, San Diego CA, March 10 – 14 2003, full paper on: www.corrosioncost.com

[14] O. Klinghoffer, T. Frolund, B. Kofoed, A. Knudsen, F.M. Jensen, T. Skovsgaard, in: J. Mietz, R. Polder, B. Elsener (Eds), Corrosion of Reinforcement in Concrete, European Federation of Corrosion, London UK (2000) p. 121

[15] F. Hunkeler, Use of stainless steel reinforcement in concrete structures, research report 543 (2000) Swiss Federal Department of the Environment, Transport, Energy and Communication (in German) download mobilityplatform.ch

[16] L. Bertolini and M. Gastaldi, Corrosion resistance of low-nickel duplex stainless steel rebars, Materials and Corrosion 62 (2011) 120 - 129

[17] B. Elsener, D. Addari, S. Coray and A. Rossi, Materials and Corrosion 62 (2011) 111 - 119

[18] A. Fahim, A. E. Dean, M.D.A. Thomas, E.G. Moffatt, Materials and Corrosion 70 (2019) 328 - 344

[19] B. Elsener and A. Rossi, Passivation of Steel and Stainless Steel in Alkaline Media Simulating Concrete, Encyclopedia of Interfacial Chemistry, Elsevier (2018) pp. 365 - 375

[20] D. Addari, B. Elsener, A. Rossi, Electrochimica Acta 53 (2008) 8078

[21] B. Elsener, S. Coray, D. Addari, A. Rossi, Electrochimica Acta 56 (2011) 4489 – 4497

[22] D. Addari, PhD Thesis University of Cagliari, 2005.

[23] S. Coray, Master Thesis, ETH Zurich and University of Cagliari, 2009.

[24] D. Büchler, B. Elsener, H. Böhni, in C.L. Page, BB. Bamdorth, J. Figg Eds, Corrosion of Reinforcement in Concrete structures, Society of Chemical Industry, London, 1966 p. 283

[25] M.P. Seah, Surf. Interface Anal. 31 (2001) 721.

[26] A. Rossi ,B. Elsener, Mater. Sci. Forum 185 – 188 (1995) 337

[27] A. Rossi, B. Elsener, Surf. Interface Anal. 18 (1992) 499.

[28] J.H. Scofield, J. Electron Spectrosc. Relat. Phenomena, 8 (1976) 129.

[29] M Fantauzzi, A Pacella, D Atzei, A Gianfagna, GB Andreozzi, A Rossi, Analytical and Bioanalytical Chemistry, 396 (2010) 2889-2898

[30] A. Rossi, G. Puddu, B. Elsener, The surface of iron and Fe10Cr alloys in alkaline media, in *Corrosion of reinforcement in concrete* ed. M. Raupach, B. Elsener, R. Polder, J. Mietz, EFC Publication Nr. 38, Woodhead Publishing (2007) p. 44.

[31] W. Fredriksson, S. Malgrem, T. Gustafsson, M. Gorgoi, K. Edström, Appl. Surf. Sci. 258 (2012) 5790 - 5797

[32] U. Nürnberger, W. Beul, Otto Graf Journal 10 (1999) 23, https://www.mpa.uni-stuttgart.de/publikationen/otto_graf_journal/ogj_1999/beitrag_nuernberger.pdf

[33] U. Angst et al., Mater Struct 50 (2017) 143

[34] U. Angst, B. Elsener, Sci Adv 3 (2017) e1700751

[35] L. Tang, J.M. Fredriksen, U. Angst, R. Polder, M. Cruz Alonso, B. Elsener, R.D. Hooton, J. Pacheco, RILEM Technical Letters 3 (2018) 25‑31

[36] C. Boschmann Käthler, U. Angst, A.M. Aguilar, B. Elsener, Corros Sci 157 (2019) 331 ‑ 336

[37] Y. Schiegg, F. Hunkeler, C.H. Voute, Use of stainless steels in concrete structures, research report 650 (2012) Swiss Federal Department of the Environment, Transport, Energy and Communication (in German) download mobilityplatform.ch